Enhanced Mass Sensing for Nanomechanical Resonators

I. De Vlaminck*, K. De Greve*, R. Naulaerts, V. Sivasubramaniam, L. Lagae, H.A.C. Tilmans, G. Borghs

IMEC, Kapeldreef 75, B-3001 Leuven, Belgium

also at ESAT/INSYS, KULEUVEN, Belgium

ABSTRACT

A new method for improving the mass detection limit of nanomechanical resonators in crystalline silicon, compatible with scaling, is demonstrated. Clamped-clamped silicon beam resonators are fabricated with a non-rectangular, 'diabolo' cross-section starting from SOI wafers. The simple, single mask process for making these resonators is demonstrated. The non-conventional cross-section results in a change of almost all functional parameters, frequency, effective mass, and signal to noise ratio, thereby decreasing the mass detection limit of the resonator up to a factor of 2.7 as compared to similar devices without the additional step. A comparison between beams with a rectangular cross-section and beams with the novel diabolo cross-section by finite element modeling confirms the predictions on frequency gain made by the analytical model. First experimental results on resonators with a rectangular and diabolo cross-section confirm the predictions made by modeling.

Keywords: nems, mass sensing, diabolo cross-section, mass detection limit.

1 INTRODUCTION

The large sensitivity of the resonance frequency of mechanical resonators to applied forces and adsorbed masses is widely exploited in sensor applications. In this context, scaling of the resonant elements has proven to be a powerful method for increasing this sensitivity. Using the scaling scheme, researchers were able to report astonishing force [1] and mass detection limits (in the attogram range and below [2,3]). These tiny mass detection limits open the doorway to an intriguing world of new biomedical applications. Further scaling of the system is expected to increase the sensitivity even more, down to single molecule mass sensitivity [4].

However, scaling limits are popping up: firstly the actuation and detection of the resonant motion of small-scale resonators becomes increasingly difficult [5], secondly the quality factor tends to deteriorate when the surface to volume ratio increases upon scaling [6].

In this communication, a new method for improving the mass sensitivity of nanomechanical resonators in crystalline silicon, compatible with scaling, will be presented. State of the art clamped-clamped silicon beam resonators are fabricated with a non-rectangular cross section starting from SOI wafers. Although the process for making these resonators differs from the standard process for making freestanding structures starting from SOI wafers [6,7] by only a single, unmasked wet etch step, almost all functional parameters are changed, thereby significantly increasing the mass sensitivity of the resonator as compared to similar devices without the additional step.

An analytical model is presented in which the parameters of importance are expressed as function of the dimensions and shape of the resonators. A detailed finite element model (FEM) study is discussed, confirming the predictions made by the analytical model on frequency gain and providing additional insight in short length effects.

The resonant behaviour of rectangular and non-rectangular resonators was studied by means of the magnetomotive method for actuation and detection.

2 FABRICATION

We use (100) silicon on insulator (SOI) wafers for fabricating all resonators. The buried oxide has a thickness of 400 nm, the silicon layer a thickness of 210 nm. The fabrication of the resonators with a non-rectangular cross-section is outlined schematically in Fig. 1A-D. Electron beam lithography is used to define the desired pattern in a polymethyl (methacrylate) resist layer. Evaporation and lift off of a Cr (10 nm)/ SiO_2 (70 nm) etch mask is performed. The pattern is transferred into the silicon by a reactive ion etch in a SF_6-O_2-Ar plasma. In regular process schemes an underetch of the sacrificial layer would conclude the resonator fabrication. In this scheme a wet, anisotropic KOH etch of the silicon is performed first. This wet etch, retarding once the (111) crystal planes are reached, defines the non-rectangular cross-section of the resonators which are aligned along the <110> direction. The Cr layer at the top and the buried SiO_2 at the bottom of the silicon provide excellent interfaces, prohibiting the silicon at the top and bottom from being attacked by the KOH solution. After the subsequent, HF-based underetching of the devices and rinsing with H_2O, acetone and isopropyl alcohol, the hard mask is removed and a layer of Al (30 nm) is deposited.

As the sidewalls of the resonator are enclosed by (111) crystal planes, a restriction is imposed on the width to thickness ratio, w/t; this ratio should be larger than cot(α) for the cross-section to be uninterrupted, 'diabolo' like (the angle between the (111) planes and the (100) planes being α = 54°7', Fig. 1C and 1D). In Fig 1E. an electron micrograph of a diabolo cross-sectioned device is shown.

We fabricated reference resonators with a rectangular cross-section using an identical process except for the wet KOH etch which is left out.

3 MODELING

The ultimate mass detection limit imposed on a nanomechanical resonator depends strongly on the dominant noise regime. Ultimate detection limits have been theoretically described for various noise sources [4,2], with the thermomechanical noise as the fundamental, measurement setup independent limit.

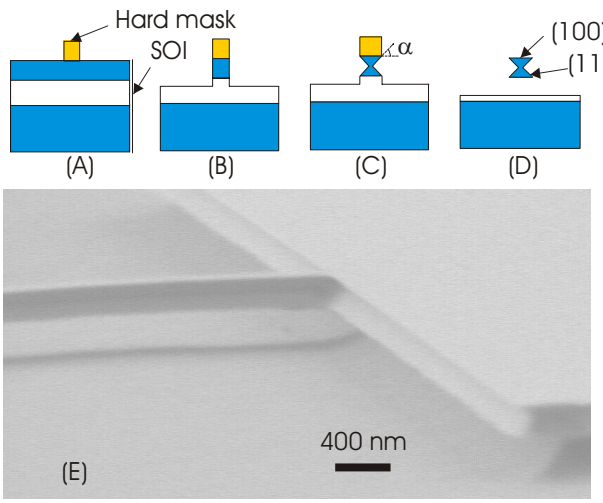

Fig. 1: Fabrication sequence of the nanomechanical resonators with the diabolo crosses section. (A) Lithographic definition of the resonator, (B) dry etch of the silicon, (C) anisotropic KOH etch, (D) removal of the hard mask and HF etch of the sacrificial silicon dioxide, (E) scanning electron micrograph of a released clamped-clamped beam resonator (0.21 X 0.21 X 12.5 μm).

The limit of detection for this thermomechanical noise limited regime can be described as [4]:

$$\delta M = 2M_{eff}\left(\frac{E_{th}}{E_c}\right)^{\frac{1}{2}}\left(\frac{\Delta f}{Q\omega_0}\right)^{\frac{1}{2}} \qquad (1)$$

where M_{eff}, E_{th}, E_c, Δf, Q, ω_0 are the effective mass, the thermal energy ($E_{th}=k_bT$), the maximum drive energy, the measurement bandwidth, quality factor, and the resonance circular frequency respectively.

The effective mass, maximum drive energy and resonance frequency can all be expressed as a function of the cross-sectional area and inertial bending moment related to the shape of the resonator. We show that the diabolo cross-section of the resonator changes all these functional parameters determining the detectable mass limit in a beneficial way compared to a resonator with the same outer dimensions and a conventional, rectangular cross-section. The cross-sectional areas (A_{rect},A_{diab}) and inertial bending moments (I_{rect},I_{diab}) corresponding to the shape and dimensions of the diabolo and rectangular beam respectively. When out of plane bending is considered these can be expressed as:

$$A_{diab} = wt - \cot(\alpha)\frac{t^2}{2}, I_{diab} = \frac{wt^3}{12} - \cot(\alpha)(\frac{t^4}{48}) \qquad (2)$$

$$A_{rect} = wt, I_{rect} = \frac{wt^3}{12}. \qquad (3)$$

If w has the minimal allowed value of $t\cdot\cot(\alpha)$ the effective area and inertial bending moment are minimal.

The effective mass M_{eff} is proportional to A, for $w= t\cdot\cot(\alpha)$ it is a factor of two smaller than for a rectangular beam.

The resonance frequency ω_0 is proportional to $\sqrt{(I/A)}$, (in the Euler-Bernoulli beam theory) [8]. Therefore the resonance frequency of the diabolo beam can be up to a factor of 1.22 higher.

The maximum signal to noise ratio, E_c/E_{th}, ($E_c= M_{eff}\omega_0^2\langle x^2\rangle$, with x the vibration amplitude) corresponds to the maximum vibration amplitude $\langle x\rangle=\langle x_{max}\rangle$ leading to a predominantly linear response. $\langle x_{max}\rangle$ is known to be proportional to $\sqrt{(I/A)}$ for a double clamped beam resonator [9], therefore E_c/E_{th} is proportional to I^2/A, for $w=t\cdot\cot(\alpha)$ it is a factor of 1.1 larger.

The quality factor is determined by the dominant energy loss mechanisms (for an overview of the various loss mechanisms we refer to ref. 10). In our case, the energy loss is assumed to be surface loss dominated, as is the case for similar sized resonators reported on in literature, which are measured under the same conditions (room temperature and low pressure). No quantitative models exist for this mechanism; therefore no shape dependencies are expressed. Looking at all proportionalities we write:

$$\frac{\delta M_{diab}}{\delta M_{rect}} \sim \left(\frac{A_{diab}}{A_{rect}}\right)^{\frac{7}{4}}\left(\frac{I_{rect}}{I_{diab}}\right)^{\frac{5}{4}}\left(\frac{Q_{rect}}{Q_{diab}}\right)^{\frac{1}{2}} \sim \kappa\left(\frac{Q_{rect}}{Q_{diab}}\right)^{\frac{1}{2}} \qquad (4)$$

$$\kappa = \left(\frac{A_{diab}}{A_{rect}}\right)^{\frac{7}{4}}\left(\frac{I_{rect}}{I_{diab}}\right)^{\frac{5}{4}} \qquad (5)$$

using (1). In Fig. 2 the quality-factor-independent ratio of mass detection limits, κ, is plotted versus w. The mass detection limit of the diabolo cross-sectioned resonator is up to a factor of 2.7 lower than for the rectangular resonator, ignoring any differences in quality factor.

3.1 Finite Element Modeling (FEM)

The analytical model for the resonance frequency used earlier was based on Euler-Bernoulli beam theory. It does not take into account rotary inertia effects and shearing deformations, nor the effect of finite stiffness of the clamping region (these effects all become increasingly important for shorter beam lengths) [8].

To investigate these effects closer, Finite Element Models were built and studied using the Msc. Marc software. A modal analysis was performed to investigate the resonance frequency of the desired resonant vibration modes. A convergence analysis was performed as to ensure relative errors were no larger than 10^{-3}.

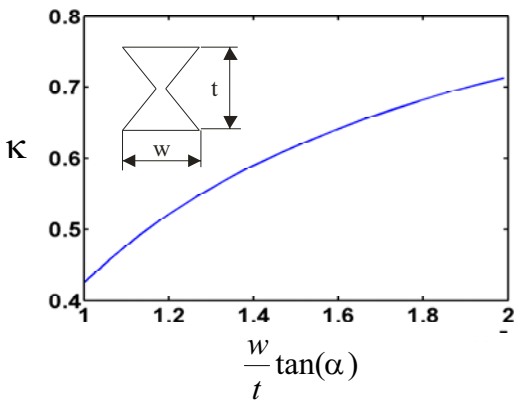

Fig. 2: κ vs. (w/t)·tan(α), (κ being the ratio of the mass detection limit of the diabolo cross-sectioned resonator and the mass detection limit of a rectangular resonator, independent of quality factor as defined in (5)).

Two different kinds of boundary conditions were imposed on both the models for the rectangular resonators and diabolo resonators. In the first the end faces of the resonator were fixed, mimicking an infinitely stiff or perfect clamping, in the second the bottom faces of the clamping region, this time included in the model, were partly fixed as to mimic a certain underetch and finite stiffness of the clamping. In Fig. 3, the models for the diabolo resonator and rectangular resonator and the different ways of modeling clamping are illustrated. The material parameters for silicon used in the calculations (taking into account the anisotropy of the material) are ρ=2330 kg/m^3, c_{11}=165 GPa, c_{12}=64 GPa, c_{44}=80 GPa.

The thickness of the resonators was chosen to be 210 nm, corresponding to the device thickness in the experiments. For resonators with a width of 150 nm (= t·cot(α)), the length was varied. In Fig. 4, the results of the FEM study are summarized and compared to the results obtained in the analytical model.

For the case of clamping with infinite stiffness, the ratio of the resonant frequencies $\omega_{diab}/\omega_{rect}$ deviates strongly from the result obtained by the analytical model ($\omega_{diab}/\omega_{rect}$=1.22) for short beam lengths. This is due to rotary inertia effects and shearing deformations, which are not taken into account in the analytical model.

The effect of rotary inertia on the resonant frequency is more outspoken for a diabolo beam than for a rectangular resonator because the rotary inertia effect is of a larger relative importance for the diabolo (again the ratio I/A), therefore the ratio of the resonant frequencies drops.

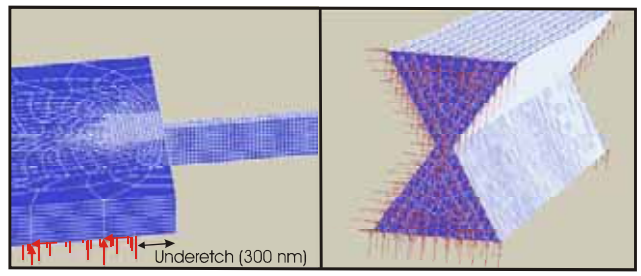

Fig. 3: (A) Model for a rectangular resonator. In this case the clamping region is included in the model. Zero-displacement boundary conditions for all directions (indicated by arrows at the nodes) are imposed at the bottom of the clamping region. Part of bottom face of the clamping region was not fixed, an underetch and finite stiffness of the clamping are mimicked as such. (B) Model for a diabolo beam resonator with the end faces fixed mimicking an infinitely stiff clamping.

In the case where the effect of finite stiffness of clamping was included in the model (underetch 300 nm), the deviation is smaller and only of importance for small and impractical beam lengths. The finite stiffness of the clamping results in a lower frequency for both rectangular and diabolo beams since part of the clamping will deform making the effective beam length larger. However this effect is less pronounced for the diabolo beam because it has a lower stiffness and will cause a smaller relative deformation of the clamping.

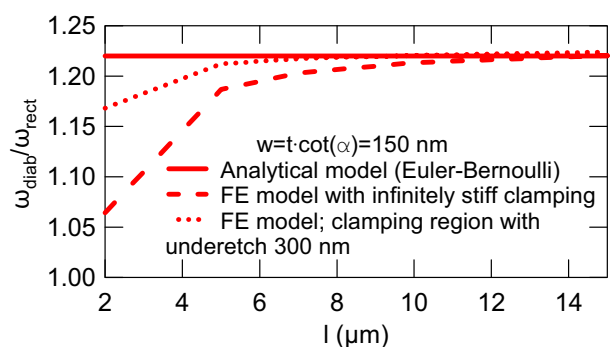

Fig.4: Comparison of the ratio $\omega_{diab}/\omega_{rect}$ calculated by the analytical and FEM models as function of beam length, l. The full line shows the result for the analytical model the dashed line shows the results for the FE models with infinite stiff clamping (indicating the effect of rotary inertia and shearing deformations), the dotted line shows the results for the FE models also including the finite stiffness of clamping (underetch 300 nm)

4 EXPERIMENTAL

Resonators with a diabolo cross-section and rectangular cross-section were fabricated using the aforementioned process schemes. The structures were made in the same process run, using the same dry etch plasma and wet etch steps except for the KOH etch which is only applied for making the diabolo cross-sectioned resonators. Before measuring the devices, we annealed them at 165°C for 12 hours. Annealing partly removes the as-deposited stress in the aluminum metal layer. An anneal-temperature dependent residual stress remains [11].

All experiments were performed using the well-described magnetomotive detection method [12]. An ac-Lorentz force acting on the resonators when applying an ac-current in a magnetic field drives the resonators. A change in resistance of the device due to oscillation in the magnetic field as function of the amplitude of vibration is sensed in a reflection based approach and provides a means of measuring the frequency spectrum. Measurements were performed at room temperature and the pressure inside the chamber was kept below 10^{-4} mbar. The applied field was 1.4 Tesla, devices were actuated out of plane in the linear operation regime.

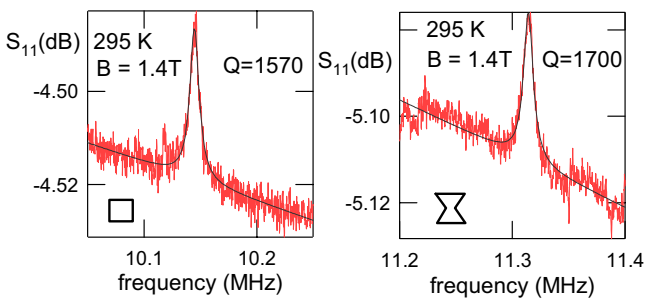

Fig. 5: frequency spectrum for a rectangular and a diabolo beam measured at room temperature and Lorentzian fit curves. Both devices have the same outer dimensions (0.23 X 0.21 X 12.5 μm). The applied field is 1.4 Tesla.

In Fig. 5 the measured frequency spectrum of a rectangular and a diabolo beam are shown. Both devices have the same outer dimensions (width 230 nm, thickness 210 nm and length 12.5 μm). The relative gain in frequency for the diabolo over the rectangular beam measured, factor 1.11, is in accordance to the expected gain for these dimensions. The surface-to-volume ratios are 0.018 nm^{-1} and 0.036 nm^{-1} for the rectangular and diabolo beam respectively. Although the surface to volume ratio is larger for the diabolo, the quality factor is slightly higher for the diabolo resonator. A thorough study towards the shape, dimension and temperature dependency of the quality factor is ongoing.

5 SUMMARY AND CONCLUSION

A novel type of nanomechanical resonator with a non-rectangular cross-section is demonstrated leading to a significantly improved mass detection limit. The fabrication process for these resonators is simple, involving a single additional, unmasked, wet etch step, and is compatible with scaling. Analytical as well as finite element modeling established that the mass detection limit can be lowered by as much as a factor of 2.7, when ignoring any changes in quality factor. First experimental results confirm the predicted gain in frequency and indicate that the quality factor is slightly higher for a diabolo shaped resonator. An elaborate study towards the shape, size and temperature dependence of the quality factor is ongoing and may provide more insight in the mechanisms governing dissipation in nanoresonators.

ACKNOWLEDGEMENT

We thank Jos Moonens and Hans Costermans for their e-beam service, Bart Vandevelde, Mario Gonzalez and Dominiek Degryse for assistance in the finite element modeling, and Johan Feyaerts and Erwin Vandenplas for technical support. IDV acknowledges financial support from the I.W.T. (Belgium), KDG acknowledges financial support from the F.W.O. (Belgium).

REFERENCES

[1] A.N. Cleland and M.L. Roukes, Nature **392**, 160 (1998).

[2] K.L. Ekinci, X.M.H. Huang and M.L. Roukes, Appl. Phys. Lett. **84**, 4469 (2004).

[3] B. Ilic, H. G. Craighead, S. Krylov, W. Senaratne, C. Ober and P. Neuzil, J. of Appl. Phys. **95**, 3694 (2004).

[4] K.L. Ekinci, Y.T. Yang, and M.L. Roukes, J. Appl. Phys **95**, 2682 (2004).

[5] M.L. Roukes, Technical digest of the 2000 Solid-State and Actuator workshop (2000), Hilton Head Isl, and SC, 4-8 June 2000

[6] D.W. Carr, S. Evoy, L. Sekaric, H.G Craighead, and J.M. Parpia, Appl. Phys. Lett. **75**, 920 (1999).

[7] S. Evoy, D.W. Carr, L. Sekaric, A. Olkhovetz, J. M. Parpia and H.G. Craighead, J. of Appl. Phys. **86**, 6072 (1999).

[8] W.J. Weaver, S.P. Timoshenko and D.H. Young, *Vibration problems in engineering* 5th Edition, Johnn Wiley & sons, New York (1990).

[9] H.A.C. Tilmans, M. Elwenspoek and J.H.J. Fluitman, Sens. actuators A **30**, 35 (1992).

[10] P. Mohanty, D. A. Harrington, K. L. Ekinci, Y. T. Yang, M. J. Murphy and M. L. Roukes, Phys. Rev. B **66**, 085416 (2002).

[11] S. Hyun, W. L. Brown and R. P. Vinci, Applied Physics Letters **83**, 4411 (2003).

[12] A. N. Cleland and M. L. Roukes, Appl. Phys. Lett. **69**, 2653 (1996).